Results in Engineering 22 (2024) 102171

Contents lists available at ScienceDirect

Results in Engineering

journal homepage: www.sciencedirect.com/journal/results-in-engineering

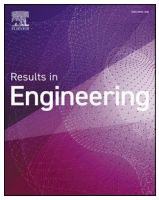

A continuum approach to multiaxial high-cycle fatigue modeling for ductile metallic materials

Sigbjørn Tveit *, Aase Reyes, Emrah Erduran

Department of Built Environment, Oslo Metropolitan University, Norway

ARTICLE INFO

Keywords:
High-cycle fatigue
Continuum approach
Hershey-Hosford function

ABSTRACT

In this work we propose a generalization of the endurance function employed in the continuum approach to high-cycle fatigue modeling by Ottosen et al. (2008). The von Mises-type backstress-modified effective stress term of the original formulation is replaced by the non-quadratic Hershey-Hosford function, which introduces flexibility with respect to the predicted fatigue limit in pure shear. While the original model assumes a fixed ratio between the fatigue limits in fully reversed torsion and fully reversed bending of 0.5774 for all materials, the modification enables the ratio to take on values on the interval from 0.5 to 0.5852 by calibration to experimental data that is readily available in the literature. Like the original formulation simplifies to the invariant-based Mises-Sines fatigue limit criterion for proportional stress histories, the current proposal can be written as a Hershey-Hosford-Sines criterion. A systematic validation to experimental multiaxial infinite fatigue life data from eight different *mild* and *semi-hard* metals with fully reversed torsion and bending fatigue limit ratios lower than 0.6 demonstrates that the proposed modification increases the accuracy and reduces the number of non-conservative predictions.

1. Introduction

The fatigue failure of structural components subjected to fluctuating loads has been the subject of extensive research since the middle of the 19th century. While Wöhler in his pioneering work [1] did the first systematic investigation on the relationship between the cyclic stress amplitude and the number of cycles at failure, Basquin [2] first represented the data in the log-log *S*–N diagram that we are familiar with today, with the stress amplitude on the ordinate and the number of cycles at failure on the abscissa. The fundamental theory of fatigue typically distinguishes between low-cycle fatigue (LCF) and high-cycle fatigue (HCF). In LCF, the fatigue crack initiation life is shorter than around 10^4 cycles, and the governing strain levels introduce plastic responses in the material. In the HCF domain, where the fatigue crack initiates at cycle numbers higher than around 10^4, the macroscopic material response is predominantly elastic. In this regime, increased fatigue lives are observed when specimens are subjected to cyclic stresses of decreasing amplitudes, until many materials display an infinite fatigue limit (also referred to as the endurance limit): a stress amplitude level at which the fatigue life is seemingly infinite, manifesting itself as a plateau in the *S*–N diagram, at around 10^6 to 10^7 cycles.

Since the early investigations, the assumption of infinite fatigue life after 10^6 to 10^7 cycles has been refuted by explorations of the very high-cycle fatigue range (VHCF) [3,4]. Yet, the existence of such a limit may appropriately be assumed for many engineering purposes. Moreover, experimental studies on the fatigue behavior of materials have revealed intricate dependencies on different configurations of static and alternating multiaxial stresses [5–7], their gradients induced by holes, notches, grooves, or surface roughness [8–10], as well as on various other factors, such as e.g. component size [11] and environmental conditions [9,12–14].

Limiting the scope to consider only the dependency on local stress histories, the stochastic nature of the phenomenon, evident from the large scatter in results reported from experimental investigations, poses a challenge to experimentalists who may rely on several parallel tests to present reliable results. Properly constructing a single fatigue limit, let alone an entire curve in the *S*–N diagram, requires several data points captured at different stress levels, including data in the range of 10^6 to 10^8 cycles. Limiting the test frequency to e.g. 20 Hz to avoid heat generation in the specimens, the time required to run a single test ranges from minutes to several days, depending on the stress amplitude. Keeping in mind that fatigue depends on the mean stress level, experimental test programs aiming to characterize the fatigue behavior of a

* Corresponding author. Post box 4, St. Olavs plass, NO-0130 Oslo, Norway.
E-mail address: sigbjorn.tveit@oslomet.no (S. Tveit).

https://doi.org/10.1016/j.rineng.2024.102171
Received 5 February 2024; Received in revised form 19 April 2024; Accepted 22 April 2024
Available online 24 April 2024

Nomenclature

A	Positive dimensionless model parameter
b_0	Infinite fatigue limit in repeated bending
b_{-1}	Infinite fatigue limit in fully reversed bending
C, K, L	Positive dimensionless model parameters
D	Fatigue damage parameter
Err	Error index
f_a	Stress amplitude scale factor
$H(x)$	Heaviside step function
h	Step size of central differentiation scheme
I_1	First invariant of the stress tensor
$I_{1,m}$	Mean value of the first stress tensor invariant of stress cycle
m	Hershey-Hosford exponent
P	Stress cycle period
R	Stress ratio of cyclic extrema
s	Deviatoric stress tensor
$s_{i,a}$	Amplitude of principal deviatoric stress tensor component of stress cycle (i $= 1, 2, 3$)
s_m	Deviatoric mean stress of stress cycle
$\widehat{s}$	Backstress-modified deviatoric stress tensor
$\widehat{s}_{ij}$	Backstress-modified deviatoric stress tensor components (i, $j = x, y, z$)
$\widehat{s}_i$	Backstress-modified deviatoric stress tensor principal components ($i = 1, 2, 3$)
S_o	Model parameter in the units of stress
t	Time variable
t_{-1}	Infinite fatigue limit in fully reversed torsion
t_f	Time at failure ($D = 1$)
x, y, z	Cartesian coordinates
$\boldsymbol{\alpha}$	Deviatoric backstress tensor
β	Endurance function
κ	Torsion-bending fatigue limit ratio
$\boldsymbol{\sigma}$	Stress tensor
$\sigma_{ij,a}$	Amplitude of stress tensor component of stress cycle
$\sigma_{ij,m}$	Mean value of stress tensor component of stress cycle
$\sigma_{e,a}$	Deviatoric effective stress amplitude of stress cycle
$\sigma_{max}, \sigma_{min}$	Maximum and minimum stress during a uniaxial cyclic stress
$\widehat{\sigma}_e$	Backstress-modified deviatoric effective stress
φ	Phase constant
ω	Angular frequency of stress cycle

certain material can easily become very comprehensive. Therefore, the material tests required for calibration of HCF models should be kept as few and simple as possible for the model to have practical application.

Considering cyclic multiaxial stress histories, the traditional concept of HCF analysis combines three model components: A fatigue limit function, a cycle counting method, and a fatigue damage accumulation law. The fatigue limit function defines the multiaxial endurance limit, separating safe from unsafe stress configurations while providing a measure of the multiaxial stress that is comparable to experimental data which typically governs uniaxial stress. Whether the fatigue limit function is formulated based on resolved stresses on material planes or invariants of the stress tensor, the input to the traditional fatigue limit functions is given in terms of cyclic mean stresses and stress amplitudes. To deal with the ambiguities that arise when the special case of constant amplitude loading does not apply, a cycle-counting method is employed [15]. The rain-flow counting technique [16] is popularly used to reduce randomly varying continuous stress histories into a finite number of discrete cycles, allowing the calculation of cyclic mean stresses and stress amplitudes for input in the fatigue limit function. Combined with a damage accumulation rule, the fatigue life may be calculated through the summation of the damage associated with each synthetic cycle.

Throughout the past century, researchers have dedicated considerable efforts to the development of models to keep up with the contemporary understanding of the phenomenological aspects of multiaxial HCF, which has continuously matured through experimental observations. The scientific progress from the Mises-based formulations for simple proportional alternating loading, to models including mean stress effects, brittleness, and non-proportionality has been critically reviewed in the literature (see e.g. Refs. [17–21]).

Despite these advancements, handling arbitrary multiaxial stress histories remains a challenge for the traditional cycle counting-based multiaxial HCF models due to their intrinsic presumption that any multiaxial stress history consists of distinct cycles. Moreover, when cycle-based analysis methods are implemented in a finite element (FE) based framework, hardware resources related to memory and storage can represent limiting factors when dealing with large or complex analysis models. Accurately identifying the cyclic stress extrema in time and space for a structure under complex loading may require high-frequency FE results to be stored, resulting in vast amounts of data for the subsequent fatigue analysis. A remedy to these issues can be to adopt a modeling approach where the damage accumulates incrementally through time, in line with concepts known from damage mechanics [22]. Since the idea of cycle-counting is disregarded, such models are able to make finite and infinite fatigue life predictions for multiaxial, variable amplitude, and even non-cyclic stress histories. An example of such a model is the continuum approach to high-cycle fatigue by Ottosen et al. [23]. In this model, a Drucker-Prager endurance surface separates stress space into a safe and an unsafe region. The fatigue damage accumulates incrementally when the stress state is located outside the surface while moving away from it. Interestingly, this results in a staircase-like damage development qualitatively similar to that seen in traditional rain-flow cycle-counting. The damage accumulates until it reaches a critical limit that corresponds to fatigue-induced material failure in the form of a macroscopic crack. During the damage development, the endurance surface follows the stress state in the deviatoric plane. As a reasonable approximation to experimental observations [24], this makes the model independent of the mean shear stress during cyclic loading, and linearly dependent on the mean normal stress through the pressure-dependent Drucker-Prager function. The model employs a total of five model parameters that are fitted to experimental fatigue data governing uniaxial stress states: two parameters dictate the shape of the endurance function, one determines the backstress evolution, and the last two parameters govern the damage development. As demonstrated by Lilja et al. [22], who implemented the model as a user-material in LS-DYNA for the complete machinery FE-based simulation of a rock drill, the continuum approach demonstrated faster integration, less data storage, and easier usage compared to the traditional cycle counting-based method. The overall agreement for variable amplitude loading was satisfactory, with the continuum approach making somewhat more conservative predictions for certain load sequences.

Since the original work was published, a number of modifications and alternative practices have been proposed to broaden the model's applicability. Ottosen et al. [25] employed the Neuber parameter to incorporate stress gradient effects, requiring only the ultimate strength of the material as additional input, and avoiding the introduction of additional calibration processes. This enhanced formulation was employed in e.g. Ref. [26], where it was coupled with FE simulations of detailed surface topographies to account for surface roughness in the calculations of fatigue crack initiation lives. Frondelius et al. [27]

adopted a classical von Mises yield criterion [28] and a nonlinear isotropic and kinematic hardening model in their effort to develop a unified continuum-based LCF and HCF model. An anisotropic expansion of the original model was proposed by Holopainen et al. [29]. Considering the privileged direction of a transversely isotropic material, they suggested a formulation where the stress tensor was decomposed into a transverse and a longitudinal part. By introducing two additional model parameters, a conditionally convex endurance function was constructed from invariants of the decomposed stress tensors. Brighenti et al. [30] employed two deviatoric and three full stress tensor invariants in their highly generalized isotropic endurance function. While the agility of this formulation is indisputable, the authors had to rely on using a genetic algorithm to tailor the total of ten model parameters to each multiaxial stress history that was considered in the study. Hence, the model does not serve the usual purpose of multiaxial fatigue models as tools to interpolate and extrapolate from relatively simple experimental tests. Multiaxial stress states were also included in the calibration method recently proposed by Ruiz et al. [31], where linear extrapolation of the stable fatigue damage development was used to avoid the mathematical challenge of developing closed-form expressions for complex cyclic stress states in the finite fatigue life regime. This allowed them to include in-phase (IP) and out-of-phase (OOP) multiaxial stress cycles in the calibration of material parameters, which reportedly enhanced the model behavior for complex stress states. Lindström [32] proposed a modification where the original Drucker-Prager type endurance function was replaced by a generalized form that carried a quadratic dependency on the first stress tensor invariant, inducing an elliptical Haigh diagram which displays better agreement with the observed mean stress dependency for ductile materials. This modified model was later coupled with the stress-gradient enhancement of Ottosen et al. [25] and implemented for an aircraft load spectrum to demonstrate the model's predictive capabilities toward experimental fatigue life data for AA7075-T6 holeplate specimens [33]. Recently, Lindström et al. [34] also applied the enhanced continuum approach [25] in the service-life assessment of integral airframes milled from plates of aluminum alloy AA7050-T7451, where they proposed yet another formulation for the dependency on hydrostatic stress. This time, conforming to the rigorous safety requirements that are requisite in aeronautical applications, a smooth unit step sigmoid function was applied to ensure conservativeness in the compression-dominated regime.

Despite these efforts to expand the application range and to improve the accuracy of the original model, to the best of our knowledge, no attempts to reformulate its governing equations to account for the relative difference between the fatigue capacities in normal stress and shear stress are found in the literature. Like in the much-employed HCF criterion of Sines [24], the original continuum approach of Ottosen et al. [23] is formulated using a deviatoric effective stress amplitude term in the fashion of von Mises [28]. The use of such a formulation implies a fixed relationship between the fully reversed fatigue limits in torsion and bending, $\kappa = 1/\sqrt{3}$ (see Eq. (6)) [17]. While this may be a reasonable approximation for steels and aluminum alloys in the lower range of the *hard* metal category ($1/\sqrt{3} \approx 0.5774 \leq \kappa \leq 0.8$), the torsion-bending fatigue limit ratio may approach 0.5 for *mild* metals, and unity for *brittle* metals [35]. Hence, models that carry the von Mises-based formulation are prone to highly conservative predictions for metals on the brittle side of the spectrum, and even non-conservative predictions for highly ductile materials.

Motivated by the empirical records of the behavior of *mild* metals, a generalization of the original continuum approach to HCF modeling [23] is presented in this study. The modified form employs a non-quadratic deviatoric effective stress term to cover *mild* and *semi-hard* metals in the range $0.5 \leq \kappa \leq 0.5852$. The new term introduces an additional model parameter whose value can be identified by a simple calibration to experimental data that is readily available in the literature for many materials. In Section 2, a summary of the original model is given, before the proposed modification is described. Section 3 describes the model's parameter calibration procedure, as well as its reduction to a simplified Hershey-Hosford-Sines criterion for proportional stress histories. In Section 4, the predictive capabilities of the original and proposed model are systematically tested towards proportional and non-proportional multiaxial experimental infinite fatigue limits for a generous selection of *mild* and *semi-hard* metals, followed by a discussion concerning the results.

2. Theory

2.1. The original continuum approach to HCF modeling

In the continuum approach to HCF, proposed by Ottosen et al. [23], a Drucker-Prager [36] endurance surface separates the stress space into two domains: a safe domain, where fatigue damage cannot develop, and an unsafe domain, where fatigue damage can develop under certain conditions. The endurance function is modified by a deviatoric backstress tensor $\boldsymbol{\alpha}$, which shifts the endurance surface in the deviatoric plane. To accumulate fatigue damage, the model employs a damage scalar. Both the backstress and the damage evolution are written in incremental form, and for their increments to be non-zero, two conditions must be fulfilled: the current stress state must be (1) located outside the endurance surface, and (2) moving away from the endurance surface in stress space.

The function β defines the endurance surface when $\beta = 0$ [23]:

$$\beta = \frac{1}{S_o}(\widehat{\sigma}_e + AI_1 - S_o) \tag{1}$$

Here, S_o is the zero-mean stress endurance limit, and A is a positive dimensionless parameter that describes the dependency on the first stress tensor invariant, $I_1 = tr(\sigma)$. Moreover, $\widehat{\sigma}_e$ is a deviatoric effective stress measure that is a function of the backstress-modified stress deviator $\widehat{\boldsymbol{s}} = \boldsymbol{s} - \boldsymbol{\alpha}$. In the fashion of von Mises [28], the deviatoric effective stress is taken as

$$\widehat{\sigma}_e = \sqrt{\frac{3}{2}}\|\widehat{\boldsymbol{s}}\| = \sqrt{\frac{(\widehat{s}_1 - \widehat{s}_2)^2 + (\widehat{s}_2 - \widehat{s}_3)^2 + (\widehat{s}_3 - \widehat{s}_1)^2}{2}} \tag{2}$$

where $\widehat{s}_1 \geq \widehat{s}_2 \geq \widehat{s}_3$ are the principal components of $\widehat{\boldsymbol{s}}$. From Eqs. (1) and (2), it follows that $\beta < 0$ corresponds to safe stress states inside the endurance locus, and $\beta > 0$ is the unsafe regime outside the surface.

The purpose of introducing a deviatoric backstress correction is to establish independence of the mean shear stress level, whose effects on fatigue are neglected in the present model. While it has been pointed out in Ref. [37] that some materials display up to 20 % reduction in the torsional fatigue limit by the presence of large mean shear stresses, this is commonly accepted as a valid approximation [17,24].

The concept is adopted from plasticity theory, where backstress tensors are used to account for the Bauschinger effect of cyclic plasticity. An obvious difference from its use in plasticity theory is the fact that the high-cycle regime governs stress states that are elastic from a macroscopic point of view. Moreover, while the stress state in a plastic process is confined to exist on a yield surface, the elastic stress state can be located outside the endurance surface in the continuum approach to HCF.

With the initial condition $\boldsymbol{\alpha}(t = 0) = 0$, the backstress tensor is written in incremental form as

$$d\boldsymbol{\alpha} = H(\beta)H(d\beta)d\beta C\widehat{\boldsymbol{s}} \tag{3}$$

where C is a positive and dimensionless model parameter, and $H(x)$ is the Heaviside step function. As $d\boldsymbol{\alpha}$ is proportional to $\widehat{\boldsymbol{s}}$, the endurance surface center will move in the direction of the current stress state in the deviatoric plane. For a cyclic stress path where the deviatoric mean stress $\boldsymbol{s}_m$ is non-zero and constant, the endurance surface will, during a

transient phase, position itself around s_m [23].

The damage scalar D exists in the continuous domain from the initial undamaged state $D(t_0) = 0$, until fatigue crack initiation at $D(t_f) = 1$. Unlike in approaches based on mesomechanics [38], the quantity cannot be directly linked to a physical phenomenon on the micro- or mesoscale in the material, and opposed to in damage mechanics where the damage variable is often related to a relative change in the elastic stiffness, the fatigue damage parameter does not influence the constitutive relation. It is written in incremental form as

$$dD = H(\beta)H(d\beta)d\beta K e^{L\beta} \tag{4}$$

By defining K and L as positive dimensionless material parameters, it is given from Eq. (4) that D is strictly increasing when $dD \neq 0$, resulting in non-recoverable damage. Note that dD is independent of the current amount of damage D, in compliance with the linear Palmgren-Miner damage accumulation hypothesis [39]. Upon access to the appropriate material data, it is possible to adopt a non-linear formulation, as was done by Kaleva et al. [40] who equipped the model with a Lemaitre-Chaboche type damage law [41]. However, the ability to compute the fatigue life by linear extrapolation of the stable damage growth [31], is then forsaken.

The incremental quantities defined in Eqs. (3) and (4) both include the endurance function increment $d\beta$, which can be obtained by differentiating β, and substituting $d\boldsymbol{\alpha}$ by the expression in Eq. (3). The endurance function increment is then expressed analytically as

$$d\beta = \frac{1}{S_0 + C\widehat{\sigma}_e}\left[\frac{3}{2}\frac{\widehat{\boldsymbol{s}} : d\boldsymbol{s}}{\widehat{\sigma}_e} + A tr(d\boldsymbol{\sigma})\right] \tag{5}$$

With this, the original continuum approach to HCF modeling provides a complete framework that complies with arbitrary stress histories, where conventional cycle-counting methods are replaced by the time-integration of the incremental expressions in Eqs. (3) and (4), using numerical integration schemes. The result is a model that combines the three elements of conventional HCF analysis in a unified event-independent formulation. For cyclic proportional stress states, the original formulation reduces to the widely used criterion of Sines [24] (hereby referred to as Mises-Sines). Consequently, the model inhibits some of the Mises-Sines criterion's limitations, such that the ratio between the fatigue limit in fully reversed torsion and bending,

$$\kappa = \frac{t_{-1}}{b_{-1}} \tag{6}$$

is confined to the value of $1/\sqrt{3} \approx 0.5774$. In the calibration procedure proposed by Ottosen et al. [23], the parameters that describe the shape of the endurance function, S_0 and A, are calibrated to normal stress fatigue limits with different mean stress levels, e.g. the fatigue limits in fully reversed and pulsating bending, b_{-1} and b_0. If b_0 is defined as the maximum absolute stress in bending for $R = \sigma_{max}/\sigma_{min} = 0$, the associated stress amplitude is $b_0/2$, which yields $S_0 = b_{-1}$ and $A = 2b_{-1}/b_0 - 1$. Intuitively, this is in line with the geometric interpretation of A as the slope of the Drucker-Prager cone. However, using single-component uniaxial fatigue limits as input for a multiaxial HCF model represents a drastic extrapolation of the experimental observations. In the application of the original Sines criterion, the parameters S_0 and A are often expressed in terms of the fatigue limits in fully reversed torsion and repeated bending, as $S_0 = \sqrt{3}t_{-1}$ and $A = 2(\sqrt{3}t_{-1} - b_0/2)/b_0$ [17]. These experimental limits are readily available in the literature for many materials, and their use provides multiaxial diversity to the calibration data, albeit at the expense of the predicted mean stress dependency in normal stress, for materials where $\kappa \neq 1/\sqrt{3}$.

In the following section, we propose a modification to the original continuum approach to HCF modeling, that for a specific range of *mild* and *semi-hard* materials allows full utilization of the three infinite fatigue limits b_{-1}, t_{-1}, and b_0.

2.2. Generalization for mild and semi-hard metals

The generalized formulation is introduced to the endurance function's dependency on the backstress-reduced deviatoric stress tensor $\widehat{\boldsymbol{s}}$. While the original endurance function employs a deviatoric term according to that of von Mises [28], the current proposal adopts the non-quadratic formulation of Hershey [42] and Hosford [43]. Keeping the original definitions given in Eqs. (1), (3) and (4), we replace Eq. (2) with

$$\widehat{\sigma}_e = \left(\frac{|\widehat{s}_1 - \widehat{s}_2|^m + |\widehat{s}_2 - \widehat{s}_3|^m + |\widehat{s}_3 - \widehat{s}_1|^m}{2}\right)^{\frac{1}{m}} \tag{7}$$

where m is the Hershey-Hosford exponent. For $m = 2$ and $m = 4$, Eq. (7) is equivalent to the von Mises formulation in Eq. (2), reducing the generalized formulation to the original one, while for $m = 1$ and $m \to \infty$, Eq. (7) is equivalent to the Tresca maximum stress criterion. The Hershey-Hosford function is commonly applied in plasticity theory and was proposed to account for crystallographic effects on the onset of yield and plastic flow in isotropic materials [44]. In such a context, m is taken as a constant that allows behavior between von Mises and Tresca in the interval $1 < m \leq 2$ (or equivalently $4 \leq m < \infty$) [44]. Particularly, it is common to use Eq. (7) with $m = 6$ and $m = 8$ to model the behavior of isotropic body-centered cubic (BCC) and face-centered cubic (FCC) materials, respectively. The domain $2 < m < 4$ is less frequently discussed in the literature. In this range, the Hershey-Hosford function takes on a form where the limit in pure shear is larger than in the von Mises formulation, with an extreme state at $m \approx 2.7670$, while remaining convex. Fig. 1 depicts the Hershey-Hosford loci in the space of normalized plane stress for various values of m.

By applying the generalized deviatoric effective stress formulation to the continuous-time fatigue model presented in Section 2.1, κ is no longer restricted to $1/\sqrt{3} \approx 0.5774$, as in the original formulation. The modification covers a range of mild metals with κ from 0.5852 at $m \approx 2.7670$, to 0.5 at $m \to \infty$. The relation between the torsion-bending fatigue limit ratio κ, and the Hershey-Hosford exponent m (see Eq. (17) in Section 3) is demonstrated in Fig. 2.

A schematic representation of the endurance surfaces for three different values of m is displayed in the positive principal stress space in Fig. 3. The white/grey surface ($m = 1.1218$) depicts the model calibrated to NiCrMo steel 75/80 ton with $\kappa = 0.5188$ [5,45] (cf. Section 4 for further information), displaying a shape close to Tresca. The light blue surface ($m = 2$) is the original Drucker-Prager cone, while the dark

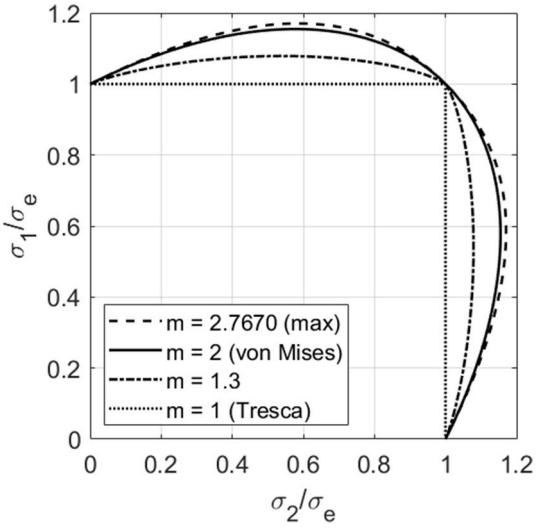

Fig. 1. Loci of the Hershey-Hosford function in the space of normalized plane stress for $\boldsymbol{\alpha} = \mathbf{0}$.

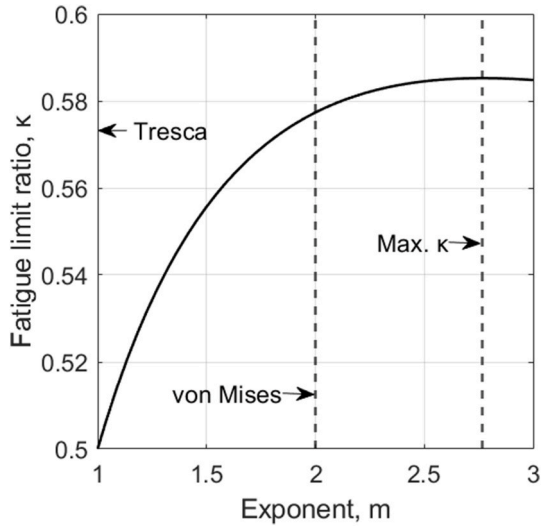

Fig. 2. Relation between the torsion-bending fatigue limit ratio κ, and the Hershey-Hosford exponent m.

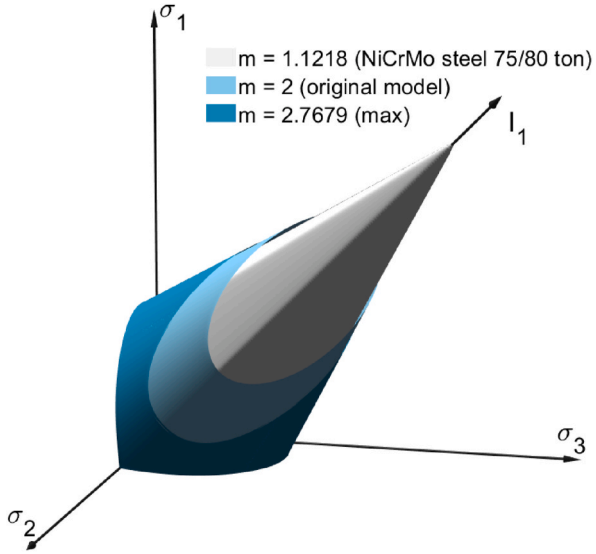

Fig. 3. Schematic representation of endurance surfaces with different Hershey-Hosford exponents, plotted in the positive principal stress space: $m = 1.1218$ (white/grey) corresponds to NiCrMo steel 75/80 ton [5,45], $m = 2$ (light blue) represents the original model, and $m = 2.7670$ (dark blue) represents the maximum exponent value (cf. Fig. 2). The latter two surfaces are intercepted by normal planes to the σ_2-axis for illustrative purposes. (For interpretation of the references to colour in this figure legend, the reader is referred to the Web version of this article.)

blue surface ($m = 2.7670$) corresponds to the maximum value of $\kappa = 0.5852$. Except for in the planes of unidirectional stress, where all the surfaces intersect, the high-exponent surfaces encapsulate the low-exponent surfaces. Thus, for illustrative purposes, the blue surfaces are intercepted by planes normal to the σ_2-axis.

To complete the modification, the new formulation of β calls for an updated expression for its increment $d\beta$, which is the driving variable of the incremental backstress $d\boldsymbol{\alpha}$, defined in Eq. (3), and the incremental damage variable dD, defined in Eq. (4). Differentiating Eq. (1) with respect to time, and substituting with the expression for $d\boldsymbol{\alpha}$ yields the general form which applies regardless the form of $\widehat{\sigma}_e$:

$$d\beta = \frac{1}{S_0 - tr\left(\left[\frac{\partial \widehat{\sigma}_e}{\partial \boldsymbol{\alpha}}\right] C[\widehat{\boldsymbol{s}}]^T\right)} \left(tr\left(\left[\frac{\partial \widehat{\sigma}_e}{\partial \boldsymbol{s}}\right][d\boldsymbol{s}]^T\right) + A\, tr(d\boldsymbol{\sigma})\right) \tag{8}$$

From the chain rule, and the definition of the backstress-reduced deviatoric stress $\widehat{\boldsymbol{s}} = \boldsymbol{s} - \boldsymbol{\alpha}$, we have

$$\frac{\partial \widehat{\sigma}_e}{\partial \boldsymbol{s}} = \frac{\partial \widehat{\sigma}_e}{\partial \widehat{\boldsymbol{s}}} \frac{\partial \widehat{\boldsymbol{s}}}{\partial \boldsymbol{s}} = \frac{\partial \widehat{\sigma}_e}{\partial \widehat{\boldsymbol{s}}} \tag{9.a}$$

$$\frac{\partial \widehat{\sigma}_e}{\partial \boldsymbol{\alpha}} = \frac{\partial \widehat{\sigma}_e}{\partial \widehat{\boldsymbol{s}}} \frac{\partial \widehat{\boldsymbol{s}}}{\partial \boldsymbol{\alpha}} = -\frac{\partial \widehat{\sigma}_e}{\partial \widehat{\boldsymbol{s}}} \tag{9.b}$$

The gradient components of $\partial \widehat{\sigma}_e / \partial \widehat{\boldsymbol{s}}$ can be expressed analytically by performing the partial derivatives using standard calculus. Alternatively, the partial derivatives may be computed through numerical differentiation. In this work, the following second-order accurate central differentiation scheme was used:

$$\frac{\partial \widehat{\sigma}_e}{\partial \widehat{s}_{xx}} \approx \frac{\widehat{\sigma}_e\left(\widehat{s}_{xx}+h, \widehat{s}_{yy}, \widehat{s}_{zz}, \widehat{s}_{xy}, \widehat{s}_{yz}, \widehat{s}_{zx}\right) - \widehat{\sigma}_e\left(\widehat{s}_{xx}-h, \widehat{s}_{yy}, \widehat{s}_{zz}, \widehat{s}_{xy}, \widehat{s}_{yz}, \widehat{s}_{zx}\right)}{2h} \tag{10.a}$$

$$\frac{\partial \widehat{\sigma}_e}{\partial \widehat{s}_{yy}} \approx \frac{\widehat{\sigma}_e\left(\widehat{s}_{xx}, \widehat{s}_{yy}+h, \widehat{s}_{zz}, \widehat{s}_{xy}, \widehat{s}_{yz}, \widehat{s}_{zx}\right) - \widehat{\sigma}_e\left(\widehat{s}_{xx}, \widehat{s}_{yy}-h, \widehat{s}_{zz}, \widehat{s}_{xy}, \widehat{s}_{yz}, \widehat{s}_{zx}\right)}{2h} \tag{10.b}$$

$$\frac{\partial \widehat{\sigma}_e}{\partial \widehat{s}_{zz}} \approx \frac{\widehat{\sigma}_e\left(\widehat{s}_{xx}, \widehat{s}_{yy}, \widehat{s}_{zz}+h, \widehat{s}_{xy}, \widehat{s}_{yz}, \widehat{s}_{zx}\right) - \widehat{\sigma}_e\left(\widehat{s}_{xx}, \widehat{s}_{yy}, \widehat{s}_{zz}-h, \widehat{s}_{xy}, \widehat{s}_{yz}, \widehat{s}_{zx}\right)}{2h} \tag{10.c}$$

$$\frac{\partial \widehat{\sigma}_e}{\partial \widehat{s}_{xy}} = \frac{\partial \widehat{\sigma}_e}{\partial \widehat{s}_{yx}} \approx \frac{\widehat{\sigma}_e\left(\widehat{s}_{xx}, \widehat{s}_{yy}, \widehat{s}_{zz}, \widehat{s}_{xy}+h, \widehat{s}_{yz}, \widehat{s}_{zx}\right) - \widehat{\sigma}_e\left(\widehat{s}_{xx}, \widehat{s}_{yy}, \widehat{s}_{zz}, \widehat{s}_{xy}-h, \widehat{s}_{yz}, \widehat{s}_{zx}\right)}{4h} \tag{10.d}$$

$$\frac{\partial \widehat{\sigma}_e}{\partial \widehat{s}_{yz}} = \frac{\partial \widehat{\sigma}_e}{\partial \widehat{s}_{zy}} \approx \frac{\widehat{\sigma}_e\left(\widehat{s}_{xx}, \widehat{s}_{yy}, \widehat{s}_{zz}, \widehat{s}_{xy}, \widehat{s}_{yz}+h, \widehat{s}_{zx}\right) - \widehat{\sigma}_e\left(\widehat{s}_{xx}, \widehat{s}_{yy}, \widehat{s}_{zz}, \widehat{s}_{xy}, \widehat{s}_{yz}-h, \widehat{s}_{zx}\right)}{4h} \tag{10.e}$$

$$\frac{\partial \widehat{\sigma}_e}{\partial \widehat{s}_{zx}} = \frac{\partial \widehat{\sigma}_e}{\partial \widehat{s}_{xz}} \approx \frac{\widehat{\sigma}_e\left(\widehat{s}_{xx}, \widehat{s}_{yy}, \widehat{s}_{zz}, \widehat{s}_{xy}, \widehat{s}_{yz}, \widehat{s}_{zx}+h\right) - \widehat{\sigma}_e\left(\widehat{s}_{xx}, \widehat{s}_{yy}, \widehat{s}_{zz}, \widehat{s}_{xy}, \widehat{s}_{yz}, \widehat{s}_{zx}-h\right)}{4h} \tag{10.f}$$

In double-precision floating-point format, a step size h in the order of 10^{-6} was found appropriate to balance the truncation error and the round-off error in the ill-conditioned differentiation scheme. Note that the partial derivatives with respect to the symmetric shear terms are calculated simultaneously and divided by two, for compliance with the matrix notation of $\partial \widehat{\sigma}_e / \partial \widehat{\boldsymbol{s}}$. This procedure also guarantees that the symmetry of the gradient is preserved. By calculating $d\beta$ according to Eq. (8)-(10), we have established the complete framework for the modified continuum approach for *mild* and *semi-hard* metals. The modified and original endurance surfaces are displayed in Fig. 4 (a) and (b) as sections in the deviatoric plane. For the specific stress increment that is illustrated, the two models display different behaviors: While $d\boldsymbol{s}$ yields an endurance function increment $d\beta > 0$ for $m = 1.1218$ in Fig. 4 (a), the same deviatoric stress increment yields $d\beta < 0$ for the original model in Fig. 4 (b).

3. Model calibration and reduction to Hershey-Hosford-Sines model

For proportional cyclic loading, it is possible to develop analytical expressions to evaluate the continuum-based model directly, which enables efficient calibration of the model parameters to experimental fatigue limits. Closed-form expressions have been developed for cyclic uniaxial tension-compression [23] and cyclic simple shear [46].

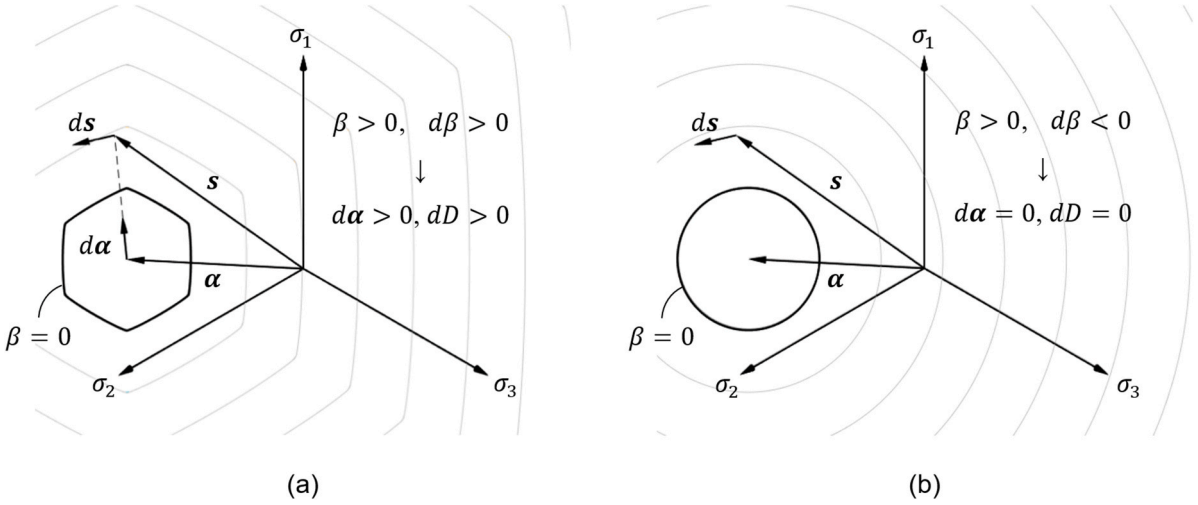

Fig. 4. State variable evolution in the deviatoric plane during a particular stress increment: (a) $m = 1.1218$ (corresponding to NiCrMo steel 75/80 ton [5,45]), (b) $m = 2$ (original model). The grey lines represent constant values of $\beta > 0$.

Just like the original formulation reduces to the invariant-based Sines criterion for proportional stress, the modification presented herein also reduces to a generalized Hershey-Hosford-Sines criterion that covers the span $0.5 \leq \kappa \leq 0.5852$. The criterion can then be expressed as an inequality where the left-hand side is the linear combination of an effective deviatoric amplitude term and a hydrostatic mean stress term:

$$\sigma_{e,a} + AI_{1,m} \leq S_0 \tag{11}$$

Here, $I_{1,m}$ is the mean of the first stress tensor and $\sigma_{e,a}$ is the Hershey-Hosford effective stress amplitude. To define the two stress terms, we consider a proportional periodic stress cycle with period P. The cyclic mean value $I_{1,m}$ is obtained as

$$I_{1,m} = \frac{1}{2}\left\{\min_{t\in P}[I_1(t)] + \max_{t\in P}[I_1(t)]\right\} \tag{12}$$

If the reduced Hershey-Hosford-Sines criterion is applied to non-proportional stress histories in a cycle counting-based framework, its amplitude $\sigma_{e,a}$ must be calculated using e.g. the concept of the minimum five-dimensional hypersphere [47]. Otherwise, the proportional stress history allows us to simply express $\sigma_{e,a}$ in terms of the principal deviatoric stress amplitudes:

$$\sigma_{e,a} = \left(\frac{|s_{1,a} - s_{2,a}|^m + |s_{2,a} - s_{3,a}|^m + |s_{3,a} - s_{1,a}|^m}{2}\right)^{\frac{1}{m}} \tag{13}$$

where $m = 2$ or 4 reduces Eq. (11) to the original Mises-Sines criterion.

As we introduce the new exponent parameter, we adhere to the approach of Ottosen et al. [23], by obtaining A and S_0 from infinite fatigue limits of uniaxial stress with different mean stress levels, further using the fatigue limit in fully reversed torsion to obtain the value of m. We start by establishing the cyclic stress histories $\sigma(t \in P)$ for the different experimental fatigue limits to obtain the expressions for $I_{1,m}$ and $\sigma_{e,a}$, from Eqs. (12) and (13).

Fully reversed bending, b_{-1}:

$$\begin{aligned} \sigma_1 &= b_{-1}\sin(\omega t) \\ \sigma_2 &= \sigma_3 = 0 \end{aligned} \quad \Rightarrow \quad \begin{aligned} \sigma_{e,a} &= b_{-1} \\ I_{1,m} &= 0 \end{aligned} \tag{14}$$

Repeated bending, b_0:

$$\begin{aligned} \sigma_1 &= b_0(1 + \sin(\omega t))/2 \\ \sigma_2 &= \sigma_3 = 0 \end{aligned} \quad \Rightarrow \quad \begin{aligned} \sigma_{e,a} &= b_0/2 \\ I_{1,m} &= b_0/2 \end{aligned} \tag{15}$$

Fully reversed torsion, t_{-1}:

$$\begin{aligned} \sigma_1 &= max\begin{bmatrix} t_{-1}\sin(\omega t) \\ -t_{-1}\sin(\omega t) \end{bmatrix} \\ \sigma_2 &= 0 \\ \sigma_3 &= min\begin{bmatrix} t_{-1}\sin(\omega t) \\ -t_{-1}\sin(\omega t) \end{bmatrix} \end{aligned} \quad \Rightarrow \quad \begin{aligned} \sigma_{e,a} &= \left[{t_{-1}}^m\left(1 + 2^{m-1}\right)\right]^{\frac{1}{m}} \\ I_{1,m} &= 0 \end{aligned} \tag{16}$$

We proceed by substituting $\sigma_{e,a}$ and $I_{1,m}$ from Eq. (14) into Eq. (11) to obtain $S_0 = b_{-1}$, and from Eq. (15) into Eq. (11) to obtain $A = 2b_{-1}/b_0 - 1$. Lastly, $\sigma_{e,a}$ and $I_{1,m}$ from Eq. (16) are substituted into Eq. (11), which gives

$$\kappa = \frac{t_{-1}}{b_{-1}} = \left(1 + 2^{m-1}\right)^{-\frac{1}{m}} \tag{17}$$

The transcendental equation above is not easily solved for m using direct methods. Hence, we apply any suitable non-linear numerical approximation technique [48] to obtain m from the input of the material parameter $0.5 \leq \kappa \leq 0.5852$. For materials with $\kappa > 0.5852$, an exponent $m = 2.7670$ can be used as a conservative approximation.

For proportional cyclic loading, it is possible to develop analytical expressions to evaluate the model directly, which enables efficient calibration of the model parameters to experimental fatigue limits. Closed-form expressions have been developed for cyclic uniaxial stresses, and because the proposed generalization does not alter the model behavior in uniaxial loading, this methodology can be directly applied to calibrate the remaining model parameters C, K, and L for application in finite fatigue life analysis. For further details regarding this, cf. Ottosen et al. [23].

4. Results and discussion

4.1. Database for experimental validation

As the endurance surface represents the infinite fatigue limit in stress space, the current proposal, which modifies the shape of this surface, was rigorously tested against multiaxial infinite fatigue life data from experimental tests on *mild* and *semi-hard* metals, adopted from the open-access FatLim database [45]. The database contains an extensive collection of infinite fatigue limit data from the literature, obtained from testing on smooth unnotched specimens subjected to combined harmonic and static loading. At the time of access (cf. [45]), the full set included a total of 551 experimental fatigue limits, distributed among 50

different materials with κ ratios from 0.5188 to 0.9490. Due to the vast collection of data collected from various sources, the experimental fatigue limits in this study were taken directly from the FatLim database, instead of consulting the primary sources. However, random checks were conducted to verify the reported values against the results published in the original source.

The majority of materials in FatLim fall within the classifications *hard* or *brittle* metals, for which the currently available continuum formulations are unsuited. To facilitate a fair trial for the fatigue models, their predictive capabilities should be tested against experimental data obtained from tests on the materials that they intend to represent; in the present case, on materials that fall within the categories of *mild* and *semi-hard* metals. The Hershey-Hosford generalization allows proper parameter fitting to materials in the range $0.5 \leq \kappa \leq 0.5852$, but also provides a better approximation for the remaining domain of κ, compared to the original model. Hence, the validation was limited to include materials with κ-ratios up to 0.6, which provided a rich experimental dataset, without extending the model's intended application range too far.

The surface stresses induced by bending and torsion during fatigue limit tests are respectively taken as measures of the fatigue limits associated with normal stress and pure shear stress. It is also possible to obtain the normal stress fatigue limit through axial push-pull tests, but the obtained measurements differ from those obtained in bending due to the effects of size and stress gradients. Although various conversion models exist [49], the present validation aims to measure the performance of the proposed modification without contamination from other models. To ensure consistency in the experimental relationship κ, the experimental data from two materials that were tested in axial push-pull were disregarded.

The resulting dataset contained 65 experimental fatigue limits for eight different ductile materials. Among these data, 16 instances corresponded to the fatigue limits in fully reversed bending (b_{-1}) and torsion (t_{-1}) of each material. Moreover, four data points were single-channel non-zero mean stress fatigue limits in either pure bending or pure torsion. The remaining 45 datapoints were multiaxial stress cycles of combined bending and torsion, out of which 35 governed in-phase loading, and 10 governed out-of-phase loading with phase differences $\varphi = 45°$, 60° or 90°.

All experimental cyclic stress states in the dataset are fully described by

$$\sigma_{xx}(t) = \sigma_{xx,m} + \sigma_{xx,a} \bullet \sin(\omega t) \tag{18.a}$$

$$\sigma_{xy}(t) = \sigma_{xy,m} + \sigma_{xy,a} \bullet \sin(\omega t - \varphi) \tag{18.b}$$

$$\sigma_{yy} = \sigma_{zz} = \sigma_{yz} = \sigma_{zx} = 0 \tag{18.c}$$

where the constants $\sigma_{xx,m}$, $\sigma_{xx,a}$, $\sigma_{xy,m}$, $\sigma_{xy,a}$, and φ of each test are reported in Appendix A, and ω is the constant angular frequency of each test.

Fig. 5 (a) exhibits all 65 experimental fatigue limits in the space of $\sigma_{xx,a}$ and $\sigma_{xy,a}$. In Fig. 5 (b) the normalized experimental datapoints that govern in-phase (\varphi = 0) combinations of fully reversed bending and torsion with zero mean stress ($\sigma_{xx,m} = \sigma_{xy,m} = 0$) are displayed, along swith the endurance limit of the original model, and the endurance limit range of the proposed generalization.

4.2. Prediction error

The model parameters are calibrated to the experimental fatigue limits, b_{-1}, b_0, and t_{-1}, which are obtained from tests on coupons reported in the literature. For each material, predictions made by the calibrated models are compared to experimental results governing multiaxial loading, on the same type of coupon. Hence, the size effect is limited to the differences among the stress distributions induced by the applied loads at the coupon level.

When evaluating fatigue models, it is common to adopt an error index considering the deviation between an experimental reference stress amplitude, and the model's prediction of the equivalent stress (see e.g. Ref. [17,18,21]). Referencing the cycle-based form in Eq. (11), this index is typically a measure of the relative difference between the left-hand side and the right-hand side of the inequality.

For the continuum-based formulation in Eq. (1), the maximum value of $S_0(1+\beta)$ during a steady-state cycle would be analogous to the left-hand side in the cycle-based formulation in Eq. (11). However, adopting an error index approach based on equivalent stress becomes inadequate due to the cyclic motion of the endurance surface in stress space. In the continuum approach, and its current modification, the parameters C, K and L govern the transient phase and the steady-state evolution during constant amplitude cyclic loading. However, only the steady-state phase has a perceptible influence on the predicted fatigue life. As pointed out in Ref. [32], in the context of parameter fitting, these three parameters co-vary to produce the same model fitness for a range of parameter sets, whereas C, which controls the transient evolution through its appearance in the incremental backstress, can be regarded as a numerical stability parameter rather than a true material parameter.

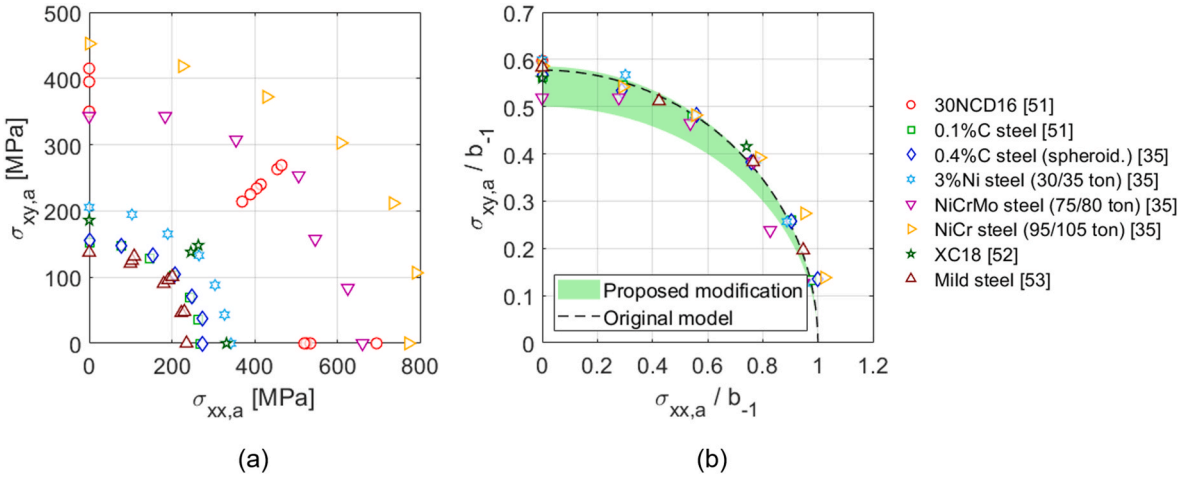

Fig. 5. Experimental fatigue limits from Ref. [45]: (a) All bending-torsion experimental tests, (b) Normalized experimental data for in-phase bending-torsion with zero mean stress, with the endurance limit of the original model (dashed), and the range of the proposed modification (green). Original publications are indicated in legend. (For interpretation of the references to colour in this figure legend, the reader is referred to the Web version of this article.)

For increasing values of C, the backstress evolution practically approaches a fully kinematic behavior where the stress state barely escapes the endurance surface during on-loading. Thus, despite that the calibrated parameter C has no link to the material on its own, it independently and significantly influences the equivalent stress measure $S_0(1+\beta)$ whenever the model prediction is conservative, resulting in falsely accurate predictions for parameter sets C, K, L with higher values of C.

To assess the model's predictive capabilities to the experimental infinite life fatigue limits in the dataset from the FatLim database, a scale factor-based error index was adopted. f_a was taken as the scale factor to the stress amplitude that causes the experimental stress state to correspond with the endurance limit. An error index in which negative values correspond to non-conservative predictions was then established as

$$Err = (1 - f_a) \bullet 100\% \tag{19}$$

To calculate Err, an algorithmic approach was used to determine f_a to a precision of less than 10^{-5} for each experimental datapoint in the dataset. For datapoints of out-of-phase stress cycles, a fourth-order Runge-Kutta numerical integration scheme [50] was employed to calculate the maximum value of β during a steady-state cycle for each trail of f_a. With reference to the above discussion, the numerical stability parameter was assigned an arbitrary high value $C = 10^4$ in all the fatigue limit calculations to ensure brevity of the transient phase. It should be further noted that the fatigue limit predictions do not require calibration of the model parameters K and L, as the fatigue damage development is irrelevant for this purpose. For datapoints of in-phase stress cycles, the closed-form solution presented in Section 3 was employed to accelerate the calculations.

Fig. 6 shows the two models' distributions of predicted errors for the experimental infinite fatigue limits in the FatLim dataset. The b_{-1} fatigue limits, which are used in the calibration of both models are excluded from the histogram data as these datapoints represent $Err = 0$ % for both models. Data representing in-phase and out-of-phase stress cycles with phase shifts of 45°, 60°, and 90° are represented with different shades in the stacked column histograms. Evident from the profiles of the plots, the proposed modification (Fig. 6 (a)) displays enhanced accuracy in comparison to the original model (Fig. 6 (b)). This is also seen in the standard deviation, which decreased from 6.87 % to 6.41 %. Out of the 57 predictions, the total number of non-conservative results was reduced from 23 to 19. This is reflected in the mean error, which is conservatively shifted from +0.222 % to +0.862 %.

The maximum absolute errors were reduced on both the conservative and the non-conservative sides, although the effect of using the proposed modification must be regarded as moderate. On the conservative side, three instances display error indices larger than +10 % for both models. These three instances are the only tests in the dataset that govern the combination of fully reversed shear stress and static normal stress, which may reveal a weakness that the models share. On the non-conservative side, the original model makes three predictions with $Err < -10$ %: two cases of out-of-phase 90° loading, and one of in-phase loading. The in-phase case represents the pure torsional fatigue limit, with $Err = -11.3$ %, and since this limit is used in the calibration of the endurance limit exponent m, the error is eliminated by using the modified formulation. The two most severe non-conservative predictions are found for cases of out-of-phase 90° loading, where the original model produced error indices of $Err = -25.8\%$ and -17.1%, and the modified model correspondingly produced $Err = -25.7\%$ and -17.1%. These instances of out-of-phase 90° loading represent stress paths that are nearly tangential to the endurance surface. It has previously been reported by Lindström et al. [46], in a study of finite fatigue lives, that the original model predicts highly non-conservative finite fatigue lives for such stress histories. After studying the model's behavior for rotary stress, they concluded that the mispredictions likely stem from the inability to predict damage accumulation for strictly tangential stress increments where $d\beta = 0$. It was suggested that a modification to the governing equations to produce nonzero damage increments under tangential stress would likely be a remedy for the shortcomings related to such stress cycles. However, in the present work, the models were tested against infinite, rather than finite fatigue limits. Under these conditions, the model depends only on the presence of a positive nonzero $d\beta$, and not on the relationship between the tangential and normal components of $d\boldsymbol{s}$. Despite this, both models predicted non-conservative error indices of considerable magnitude for the near-tangential stress histories. This result indicates that a modification based on the approach theorized in the discussion of Lindström et al. [46] would not fully solve the model's issues related to rotary stress cycles.

Although the continuum approach to high-cycle fatigue is capable of considering both finite and infinite fatigue lives, the experimental validation presented here governed only infinite fatigue limits. Upon access to experimental S–N curves for bending, torsion, and combined bending-torsion, it would have been possible to also validate the models' extrapolation capabilities to the finite fatigue life domain. Unfortunately, to the best of the authors' knowledge, such experimental data do not exist in the literature for the materials in question. Nevertheless, since the parameters of the endurance function are entirely defined in terms of infinite fatigue life data, testing the models' interpolation

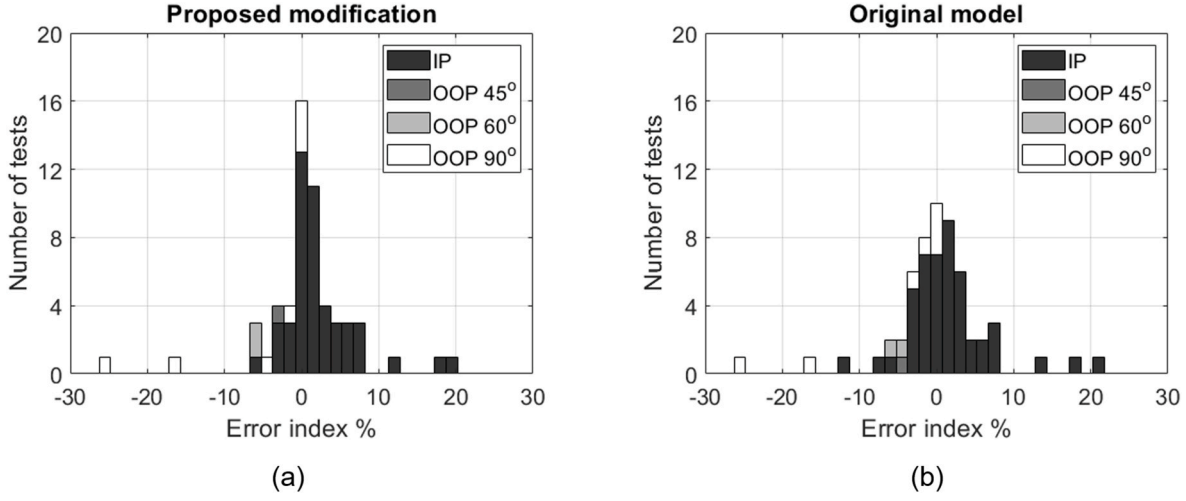

Fig. 6. Histogram of stacked columns displaying predicted errors to the experimental data in the dataset from FatLim for (a) the proposed modification, and (b) the original model.

capabilities towards a rich database of infinite fatigue life data is considered to be a solid validation of the proposed modification. The analysis demonstrates that the proposed modification is an enhancement of the original model, which increases the model's accuracy for shear stress-dominated stress paths. The model's application requires only minor alterations to the original implementation, and the new exponent parameter m is easily calibrated to experimental data without interfering with the other model parameters. The fact that the modification only affects the deviatoric term in β, also allows it to be used in conjunction with other alternative formulations, such as the mean stress modifications proposed by Lindström et al. [32,34].

5. Conclusion

This study presents a generalization of the continuum approach to high-cycle fatigue modeling by Ottosen et al. [23], with applications for *mild* and *semi-hard* materials. To overcome the original model's inherent implication that the ratio between the fatigue limits in fully reversed torsion and bending is $1/\sqrt{3} \approx 0.5774$ for all materials, a modification was introduced to the backstress-reduced deviatoric effective stress term, where the von Mises-like function of the original model was replaced by a generalized non-quadratic formulation that holds an exponent model parameter. An analytical relationship was established between the exponent parameter and the torsion-bending fatigue limit ratio, which facilitates the model's calibration to materials with torsion-bending fatigue limit ratios between 0.5 and 0.5852. In the same way that the original model reduces to the Mises-Sines criterion for proportional stress histories, the proposed modification reduces to a new Hershey-Hosford-Sines fatigue limit criterion, which has practical applications beyond its use in the continuum approach. This is a first step to solving the problem related to the fixed torsion-bending fatigue limit ratio, and proof that alternative deviatoric functions can be applied to solve the issue.

The continuum-based models were systematically validated towards multiaxial experimental infinite fatigue limits from eight different materials with torsion-bending fatigue limit ratios between 0.5 and 0.6. Application of the modified formulation resulted in increased accuracy in the prediction of the multiaxial fatigue limit, reducing the error standard deviation, the absolute extremal errors, as well as the total number of non-conservative predictions. Although the overall improvement was rather moderate, the enhancement was more significant for highly ductile materials where the torsion-bending fatigue limits were close to 0.5. This was illustrated by the predictions made for a NiCrMo 75/80-ton steel, where non-conservative prediction errors of up to 11.3 % were eliminated by using the modified formulation.

There is potential for improvement through further research as both models seem to underestimate the fatigue capacity for stress cycles of combined fully reversed shear stress and static normal stress, and overestimate the fatigue capacity for out-of-phase bending and torsion with phase differences of 90° where the stress paths are near-tangential to the endurance surface. To model the behavior of materials that display sensitivity to changes in the cyclic mean shear stress requires a revised formulation of the backstress evolution. Further experimental work is required to construct full S–N curves in bending, torsion, and combined bending-torsion for ductile materials, to study the accuracy of the models in the finite fatigue life domain.

In this work, the fatigue limits in bending and torsion were directly taken as the fatigue limits in normal and shear stress, respectively, disregarding the effects of stress gradients. In Ref. [25], Ottosen et al. present an enhanced form of the continuum approach to high-cycle fatigue which considers stress gradient effects through simple modifications of the model parameters, where the triaxial relative stress gradient is defined using an effective stress term on the von Mises form. While the implementation of this extension is straightforward for the generalized model proposed herein, future work should investigate whether the formulation of the triaxial relative stress gradient could employ a non-quadratic effective stress term as well. Furthermore, efforts are dedicated towards a modification to the continuum approach of high-cycle fatigue that covers the remaining domain of the torsion-bending fatigue limit ratios from 0.5852 to 1, in order to accurately model the behavior of *brittle* metallic material.

CRediT authorship contribution statement

Sigbjørn Tveit: Writing – original draft, Visualization, Validation, Software, Project administration, Methodology, Investigation, Formal analysis, Data curation, Conceptualization. **Aase Reyes:** Writing – review & editing, Supervision, Project administration, Methodology, Funding acquisition. **Emrah Erduran:** Writing – review & editing, Supervision, Methodology.

Declaration of competing interest

The authors declare that they have no known competing financial interests or personal relationships that could have appeared to influence the work reported in this paper.

Data availability

The data that was used in the research is rendered in completion in the manuscript's appendix.

Acknowledgments

The present work was carried out with financial support from the Faculty of Technology, Arts and Design, Oslo Metropolitan University. The authors express their gratitude to Prof. Niels Saabye Ottosen for valuable discussions during the last stages of the publication process.

Appendix A. Experimental validation data

The dataset from FatLim that was used in the experimental validation in Section 4 is reproduced in Table A.1, along with the primary source, the associated calibrated model parameters, and the prediction errors of the original model and the proposed modification.

Table A.1
Experimental validation: Dataset [45], model parameters, and prediction errors.

Material	Prim. source	$\sigma_{xx,a}$	$\sigma_{xx,m}$	$\sigma_{xy,a}$	$\sigma_{xy,m}$	φ	b_{-1}	t_{-1}	κ	S_0	A	m	*Err* Mod.	*Err* Orig.
		[MPa]	[MPa]	[MPa]	[MPa]	[°]	[MPa]	[MPa]	[−]	[MPa]	[−]	[−]	[%]	[%]
30NCD16	[51]	550	450	0	0	0	695	415	0.5971	695	0.3365	2.7670	1.17	1.17
		525	510	0	0	0							0.31	0.31
		535	600	0	0	0							7.84	7.84
		0	300	395	0	0							12.0	13.2

(*continued on next page*)

Table A.1 (*continued*)

Material	Prim. source	$\sigma_{xx,a}$ [MPa]	$\sigma_{xx,m}$ [MPa]	$\sigma_{xy,a}$ [MPa]	$\sigma_{xy,m}$ [MPa]	φ [°]	b_{-1} [MPa]	t_{-1} [MPa]	κ [−]	S_0 [MPa]	A [−]	m [−]	*Err* Mod. [%]	*Err* Orig. [%]
		455	300	263	200	0							7.40	7.74
		465	300	269	200	90							0.00	0.00
		0	450	395	0	0							19.5	20.6
		415	450	240	0	0							7.12	7.46
		405	450	234	0	90							0.00	0.00
		0	600	350	0	0							17.6	18.7
		370	600	214	0	0							5.51	5.85
		390	600	225	0	90							0.00	0.00
		0	0	415	0	0							1.99	3.31
		520	520	0	0	0							0.00	0.00
0.1%C steel	[35]	262.6	0	35.5	0	0	268.7	151.4	0.5635	268.7	-	1.6304	0.40	0.37
		242.5	0	69.5	0	0							1.00	0.75
		205.4	0	103.5	0	0							2.20	1.44
		146.7	0	128.2	0	0							0.53	−0.97
		78.8	0	146.7	0	0							1.15	−1.00
		0	0	151.4	0	0							0.00	−2.47
0.4%C steel (spheroid.)	[35]	274.9	0	37.1	0	0	274.9	156.0	0.5675	274.9	-	1.7128	2.64	2.63
		248.7	0	71.0	0	0							1.07	0.92
		208.5	0	105.0	0	0							1.16	0.64
		154.4	0	132.8	0	0							1.78	0.77
		78.8	0	146.7	0	0							−1.78	−3.33
		0	0	156.0	0	0							0.00	−1.74
3%Ni steel (30/35 ton)	[35]	327.4	0	43.2	0	0	342.9	205.4	0.5990	342.9	-	2.7670	−2.11	−2.10
		304.3	0	88.0	0	0							−0.82	−0.75
		265.6	0	132.8	0	0							2.14	2.41
		190.0	0	165.3	0	0							−0.47	0.21
		103.5	0	194.6	0	0							1.63	2.75
		0	0	205.4	0	0							2.30	3.62
NiCrMo steel (75/80 ton)	[35]	625.5	0	83.4	0	0	661.0	342.9	0.5188	661.0	-	1.1218	−2.50	−2.97
		546.7	0	157.5	0	0							−6.02	−8.19
		506.6	0	253.3	0	0							5.77	1.37
		355.2	0	307.3	0	0							4.12	−3.30
		183.8	0	342.9	0	0							3.60	−6.32
		0	0	342.9	0	0							0.00	−11.3
NiCr steel (95/105 ton)	[35]	790.7	0	106.6	0	0	772.2	452.5	0.5860	772.2	-	2.7670	4.89	4.90
		735.1	0	211.6	0	0							5.93	5.99
		608.5	0	302.7	0	0							3.60	3.86
		429.4	0	372.2	0	0							−0.37	0.31
		225.5	0	418.5	0	0							−2.89	−1.72
		0	0	452.5	0	0							0.13	1.47
XC18	[52]	246	0	138	0	0	332	186	0.5602	332	-	1.5727	4.31	3.21
		246	0	138	0	45							−3.18	−4.21
		264	0	148	0	90							−25.7	−25.8
		0	0	186	0	0							0.00	−3.05
Mild steel	[53]	222.9	0	46.2	0	0	235.4	137.3	0.5833	235.4	-	2.3445	0.58	0.60
		180.2	0	90.1	0	0							1.02	1.25
		99.8	0	120.5	0	0							−2.48	−1.75
		191.3	0	95.7	0	60							−6.67	−6.52
		103.6	0	125.0	0	60							−5.47	−4.73
		230.2	0	47.7	0	90							−1.69	−1.77
		201.0	0	100.5	0	90							−17.1	−17.1
		108.9	0	131.4	0	90							−3.99	−2.87
		0	0	137.3	0	0							0.00	1.01

References

[1] A. Wöhler, Wöhler's experiments on the strength of metals, Engineering 4 (1867) 160–161.

[2] O.H. Basquin, The exponential law of endurance tests, Proc Am Soc Test Mater 10 (1910) 625–630.

[3] T. Sakai, Historical review and future prospect for researches on very high cycle fatigue of metallic materials, Fatig. Fract. Eng. Mater. Struct. 46 (2023) 1217–1255, https://doi.org/10.1111/ffe.13885.

[4] T. Sakai, Review and prospects for current studies on very high cycle fatigue of metallic materials for machine structural use, Journal of solid mechanics and materials engineering 3 (2009) 425–439, https://doi.org/10.1299/jmmp.3.425.

[5] H.J. Gough, H. Pollard, W. Clenshaw, Some Experiments on the Resistance of Metals to Fatigue under Combined Stresses, 1951.

[6] R. Tovo, P. Lazzarin, F. Berto, M. Cova, E. Maggiolini, Experimental investigation of the multiaxial fatigue strength of ductile cast iron, Theor. Appl. Fract. Mech. 73 (2014) 60–67, https://doi.org/10.1016/j.tafmec.2014.07.003.

[7] J. Li, X. Wang, K. Li, Yy Qiu, A modification of Matake criterion for considering the effect of mean shear stress under high cycle fatigue loading, Fatig. Fract. Eng. Mater. Struct. 44 (2021) 1760–1782, https://doi.org/10.1111/ffe.13458.

[8] S.-P. Zhu, W.-L. Ye, J.A.F.O. Correia, A.M.P. Jesus, Q. Wang, Stress gradient effect in metal fatigue: review and solutions, Theor. Appl. Fract. Mech. 121 (2022) 103513, https://doi.org/10.1016/j.tafmec.2022.103513.

[9] J.Z. He, J.N. Lu, X.Y. Deng, X.Q. Xing, Z.C. Luo, Premature fracture of high-strength suspension springs caused by corrosion fatigue cracking, Results in Engineering 16 (2022) 100749, https://doi.org/10.1016/j.rineng.2022.100749.

[10] Q.M. Zobaer Shah, M.A. Chowdhury, M.A. Kowser, The aspect of the corrosion pitting with fretting fatigue on Aluminum Alloy: a nuclear reactor safety or an aerospace structural failure phenomenon, Results in Engineering 15 (2022) 100483, https://doi.org/10.1016/j.rineng.2022.100483.

[11] S.-P. Zhu, Y. Ai, D. Liao, J.A.F.O. Correia, A.M.P. De Jesus, Q. Wang, Recent advances on size effect in metal fatigue under defects: a review, Int. J. Fract. 234 (2022) 21–43, https://doi.org/10.1007/s10704-021-00526-x.

[12] T. Kieczka, E. Kerscher, Investigation of the fatigue behavior of AlMg4. 5Mn (EN AW-5083) in the temperature range-60 C< T< 20 C, Mater. Sci. Forum 690 (2011) 290–293. https://doi.org/10.4028/www.scientific.net/MSF.690.290.

[13] K. Mutombo, M. du Toit, Corrosion fatigue behaviour of aluminium alloy 6061-T651 welded using fully automatic gas metal arc welding and ER5183 filler alloy, Int. J. Fatig. 33 (2011) 1539–1547, https://doi.org/10.1016/j.ijfatigue.2011.06.012.
[14] S. Sen, H. Li, L. Khazanovich, Effect of climate change and urban heat islands on the deterioration of concrete roads, Results in Engineering 16 (2022) 100736, https://doi.org/10.1016/j.rineng.2022.100736.
[15] R. Sunder, S.A. Seetharam, T.A. Bhaskaran, Cycle counting for fatigue crack growth analysis, Int. J. Fatig. 6 (1984) 147–156, https://doi.org/10.1016/0142-1123(84)90032-X.
[16] M. Matsuishi, T. Endo, Fatigue of metals subjected to varying stress, in: Japan Society of Mechanical Engineers, 1968, pp. 37–40. Fukuoka, Japan.
[17] I.V. Papadopoulos, P. Davoli, C. Gorla, M. Filippini, A. Bernasconi, A comparative study of multiaxial high-cycle fatigue criteria for metals, Int. J. Fatig. 19 (1997) 219–235, https://doi.org/10.1016/S0142-1123(96)00064-3.
[18] J. Papuga, A survey on evaluating the fatigue limit under multiaxial loading, Int. J. Fatig. 33 (2011) 153–165, https://doi.org/10.1016/j.ijfatigue.2010.08.001.
[19] B. Kenmeugne, B. Soh Fotsing, G. Anago, M. Fogue, J. Robert, J. Kenne, On the evolution and comparison of multiaxial fatigue criteria, Int. J. Eng. Technol. 4 (2012) 37–46.
[20] M. de Freitas, Multiaxial fatigue: from materials testing to life prediction, Theor. Appl. Fract. Mech. 92 (2017) 360–372, https://doi.org/10.1016/j.tafmec.2017.05.008.
[21] Ø.A. Bruun, G. Härkegård, A comparative study of design code criteria for prediction of the fatigue limit under in-phase and out-of-phase tension–torsion cycles, Int. J. Fatig. 73 (2015) 1–16, https://doi.org/10.1016/j.ijfatigue.2014.10.015.
[22] M. Lilja, J. Karlsson, A. Jonsson, D. Hilding, S.B. Lindström, D. Leidermark, et al., Incremental damage model for fatigue life assessment in complete machinery simulation, in: 16th International LS-DYNA Users Conference, 2020.
[23] N.S. Ottosen, R. Stenstrom, M. Ristinmaa, Continuum approach to high-cycle fatigue modeling, Int. J. Fatig. 30 (2008) 996–1006, https://doi.org/10.1016/j.ijfatigue.2007.08.009.
[24] G. Sines, Failure of Materials under Combined Repeated Stresses with Superimposed Static Stresses, Univ., Los Angeles, 1955. California.
[25] N.S. Ottosen, M. Ristinmaa, R. Kouhia, Enhanced multiaxial fatigue criterion that considers stress gradient effects, Int. J. Fatig. 116 (2018) 128–139, https://doi.org/10.1016/j.ijfatigue.2018.05.024.
[26] B. Skallerud, S.K. As, N.S. Ottosen, A gradient-based multiaxial criterion for fatigue crack initiation prediction in components with surface roughness, Int. J. Fatig. 117 (2018) 384–395, https://doi.org/10.1016/j.ijfatigue.2018.08.020.
[27] T. Frondelius, S. Holopainen, R. Kouhia, N.S. Ottosen, M. Ristinmaa, J. Vaara, A continuum based macroscopic unified low-and high cycle fatigue model, in: ICMFF12-12th International Conference on Multiaxial Fatigue and Fracture, EDP Sciences, 2019.
[28] R. von Mises, On Saint Venant's Principle, 1945.
[29] S. Holopainen, R. Kouhia, T. Saksala, Continuum approach for modelling transversely isotropic high-cycle fatigue, Eur. J. Mech. Solid. 60 (2016) 183–195, https://doi.org/10.1016/j.euromechsol.2016.06.007.
[30] R. Brighenti, A. Carpinteri, S. Vantadori, Fatigue life assessment under a complex multiaxial load history: an approach based on damage mechanics, Fatig. Fract. Eng. Mater. Struct. 35 (2012) 141–153, https://doi.org/10.1111/j.1460-2695.2011.01600.x.
[31] A. Rubio Ruiz, T. Saksala, D. Baroudi, M. Hokka, R. Kouhia, High-cycle fatigue model calibration with a deterministic optimization approach, Int. J. Fatig. 175 (2023) 107747, https://doi.org/10.1016/j.ijfatigue.2023.107747.
[32] S.B. Lindstrom, Continuous-time, high-cycle fatigue model for nonproportional stress with validation for 7075-T6 aluminum alloy, Int. J. Fatig. 140 (2020), https://doi.org/10.1016/j.ijfatigue.2020.105839.
[33] S.B. Lindström, J. Moverare, D. Leidermark, H. Ansell, Z. Kapidžić, Incremental fatigue damage modeling of 7050-T7 aluminum alloy at stress-raisers, Int. J. Fatig. 161 (2022) 106878, https://doi.org/10.1016/j.ijfatigue.2022.106878.
[34] S.B. Lindström, J. Moverare, J. Xu, D. Leidermark, R. Eriksson, H. Ansell, et al., Service-life assessment of aircraft integral structures based on incremental fatigue damage modeling, Int. J. Fatig. 172 (2023) 107600, https://doi.org/10.1016/j.ijfatigue.2023.107600.
[35] H.J. Gough, H.V. Pollard, The strength of metals under combined alternating stresses, Proc. Inst. Mech. Eng. 131 (1935) 3–103, https://doi.org/10.1243/pime_proc_1935_131_008_02.
[36] D.C. Drucker, W. Prager, Soil mechanics and plastic analysis or limit design, Q. Appl. Math. 10 (1952) 157–165.
[37] J. Papuga, R. Halama, Mean stress effect in multiaxial fatigue limit criteria, Arch. Appl. Mech. 89 (2019) 823–834, https://doi.org/10.1007/s00419-018-1421-7.
[38] K. Dang-Van, Macro-Micro Approach in High-Cycle Multiaxial Fatigue, ASTM International, 1993.
[39] M.A. Miner, Cumulative Damage in Fatigue, 1945.
[40] O. Kaleva, H. Orelma, D. Petukhov, Parameter estimation of a high-cycle fatigue model combining the Ottosen-Stenstrom-Ristinmaa approach and Lemaitre-Chaboche damage rule, Int. J. Fatig. 147 (2021), https://doi.org/10.1016/j.ijfatigue.2021.106153.
[41] J. Lemaitre, J.-L. Chaboche, Mechanics of Solid Materials, Cambridge University Press, 1994.
[42] A.V. Hershey, The Elasticity of an isotropic Aggregate of anisotropic cubic Crystals, J. Appl. Mech. 21 (1954) 236–240, https://doi.org/10.1115/1.4010899.
[43] W.F. Hosford, A generalized isotropic yield criterion, J. Appl. Mech. 39 (1972) 607–609.
[44] W.F. Hosford, On the crystallographic basis of yield criteria, Textures Microstruct. 26 (1970).
[45] Papuga J. FatLim database. www.pragtic.com/experiments.php [accessed 27 November 2023].
[46] S.B. Lindstrom, C.J. Thore, S. Suresh, A. Klarbring, Continuous-time, high-cycle fatigue model: Validity range and computational acceleration for cyclic stress, Int. J. Fatig. 136 (2020), https://doi.org/10.1016/j.ijfatigue.2020.105582.
[47] I. Papadopoulos, Fatigue polycyclique des métaux: une nouvelle approche, École nationale des ponts et chaussées, 1987.
[48] R.P. Brent, Algorithms for minimization without derivatives, Courier Corporation (2013) 19–112.
[49] P. Strzelecki, T. Tomaszewski, Analysis of axial load and bending load effects on the fatigue life, in: AIP Conference Proceedings, AIP Publishing, 2018.
[50] W. Kutta, Beitrag zur näherungsweisen Integration totaler Differentialgleichungen, Teubner, 1901.
[51] C. Froustey, S. Lasserre, Fatigue des aciers sous sollicitations combinees application a l'acier 30 NCD 16. Laboratoire Arts et Metiers d'Etude de la Fatigue, 1988.
[52] A. Galtier, Contribution à l'étude de l'endommagement des aciers sous sollicitations uni ou multi-axiales, ENSAM, Paris, 1993.
[53] T. Nishihara, M. Kawamoto, The Strength of Metals under Combined Alternating Bending and Torsion with Phase Difference, vol. 11, Memoirs of the College of Engineering, Kyoto Imperial University, 1945, pp. 85–112.